


RESEARCH ARTICLE

Identification of essential tremor based on resting-state functional connectivity

Xueyan Zhang¹  | Huiyue Chen¹ | Xiaoyu Zhang¹ | Hansheng Wang¹ | Li Tao¹ | Wanlin He¹ | Qin Li¹ | Oumei Cheng² | Jing Luo² | Yun Man² | Zheng Xiao² | Weidong Fang¹

¹Department of Radiology, The First Affiliated Hospital of Chongqing Medical University, Chongqing, China

²Department of Neurology, The First Affiliated Hospital of Chongqing Medical University, Chongqing, China

Correspondence

Weidong Fang, Department of Radiology, The First Affiliated Hospital of Chongqing Medical University, No. 1 Youyi Road, Yuzhong District, Chongqing 400016, China.
Email: fwd9707@sina.com

Funding information

National Natural Science Foundation of China, Grant/Award Number: 81671663; Natural Science Foundation of Chongqing, Grant/Award Number: cstc2014jcyjA10047

Abstract

Currently, machine-learning algorithms have been considered the most promising approach to reach a clinical diagnosis at the individual level. This study aimed to investigate whether the whole-brain resting-state functional connectivity (RSFC) metrics combined with machine-learning algorithms could be used to identify essential tremor (ET) patients from healthy controls (HCs) and further revealed ET-related brain network pathogenesis to establish the potential diagnostic biomarkers. The RSFC metrics obtained from 127 ET patients and 120 HCs were used as input features, then the Mann-Whitney *U* test and the least absolute shrinkage and selection operator (LASSO) methods were applied to reduce feature dimensionality. Four machine-learning algorithms were adopted to identify ET from HCs. The accuracy, sensitivity, specificity and the area under the curve (AUC) were used to evaluate the classification performances. The support vector machine, gradient boosting decision tree, random forest and Gaussian naïve Bayes algorithms could achieve good classification performances with accuracy at 82.8%, 79.4%, 78.9% and 72.4%, respectively. The most discriminative features were primarily located in the cerebello-thalamo-motor and non-motor circuits. Correlation analysis showed that two RSFC features were positively correlated with tremor frequency and four RSFC features were negatively correlated with tremor severity. The present study demonstrated that combining the RSFC matrices with multiple machine-learning algorithms could not only achieve high classification accuracy for discriminating ET patients from HCs but also help us to reveal the potential brain network pathogenesis in ET.

KEYWORDS

classification, essential tremor, functional magnetic resonance imaging, machine learning, resting-state functional connectivity

Xueyan Zhang and Huiyue Chen contributed equally to this study.

This is an open access article under the terms of the [Creative Commons Attribution-NonCommercial-NoDerivs](https://creativecommons.org/licenses/by-nc-nd/4.0/) License, which permits use and distribution in any medium, provided the original work is properly cited, the use is non-commercial and no modifications or adaptations are made.

© 2022 The Authors. *Human Brain Mapping* published by Wiley Periodicals LLC.

1 | INTRODUCTION

Essential tremor (ET) is one of the most prevalent movement disorders and is clinically characterized by kinetic or postural tremor in bilateral upper limbs (Reich, 2019). Although growing evidence pointed out that abnormalities in the cerebello-thalamo-cortical pathway were related to ET patients (Nicoletti et al., 2020), the etiology, pathology and brain network pathogenesis mechanisms underlying ET are still surprisingly enigmatic. Due to the lack of objective neurobiological biomarkers, clinicians rely primarily on clinical symptoms to diagnose ET and conventional magnetic resonance imaging (MRI) is usually performed to rule out other tremor diseases, such as stroke and head trauma causing the tremor.

Over the past decade, resting-state functional MRI (Rs-fMRI) with blood oxygenation level-dependent (BOLD) signal has emerged as the most promising method to study brain network pathogenesis mechanisms in various neurologic diseases, including neurodegenerative diseases and ET. Using seed-based functional connectivity (FC) (Fang et al., 2016), local FC (Fang et al., 2013), global FC (Tsuboi et al., 2021) and graph theory (Benito-Leon et al., 2019) analysis of Rs-fMRI, our previous studies and those of other scholars have revealed that FC or brain network topological properties changes in the cerebello-thalamo-cortical network were associated with ET patients. However, all these above studies were traditionally mass univariate analyses at the group level that could not be used to diagnose individual ET patients. Fortunately, this shortage has been complemented by machine-learning algorithms (Pereira et al., 2009). It can establish optimal models for classification by learning and training from a large-scale complex input dataset and the model is a tool to infer the label of a new single subject (Norman et al., 2006). Using brain gray matter volume and cortical thickness as input features, machine-learning algorithms could achieve good classification performance to identify orthostatic tremor from ET with an accuracy of 100% (Benito-León et al., 2019). Another research employing cerebellar gray matter volumes and cerebellar peduncles white matter volumes as input features could discriminate ET from healthy controls (HCs) with a test accuracy at 86.66% (Prasad et al., 2019). However, up till now, using the resting-state FC (RSFC) matrices as input features for machine-learning algorithms to discriminate ET from HCs has not been investigated.

In the present study, we combined RSFC matrices with multiple machine-learning algorithms to explore whether whole-brain RSFC values could serve as high-power discriminating features for identifying ET from HCs. We hypothesized that these multiple machine-learning algorithms could achieve good classification performances, and these significant discriminative features would further help us understand the underlying brain network pathogenesis mechanisms in ET patients.

2 | METHODS AND MATERIALS

2.1 | Participants and clinical evaluation

All ET patients included in this study were recruited at the movement disorders outpatient clinic of the First Affiliated Hospital of

Chongqing Medical University. HCs were recruited from the local area through an open advertisement, and evaluated by experienced neurologists. All participants underwent medical history collection, neuropsychiatric evaluation, and MRI scans. The inclusion criteria for subjects were as follows: (1) ET patients were diagnosed by two movement specialists (OM C, and Z X) in terms of the 2018 Consensus Criteria of the Movement Disorder Society (Bhatia et al., 2018), and all ET patients had annual follow-ups through the outpatient department or by telephone; (2) the patients had an onset age between 18 and 55 years old, and patients with earlier or later onset were not included; (3) the patients were without any apparent cognitive impairment (Mini-Mental State Examination [MMSE] scores >24) and were right-handed; (4) the patients presented with moderate or greater amplitude kinetic tremor (tremor rating ≥ 2 during at least three tests); (5) patients were excluded in this study if they complied with the diagnosis of Parkinson's disease (PD), secondary causes of PD (such as Parkinsonism), dystonia, and tremor of other origins (such as stroke, tumor and trauma); (6) HCs were excluded if they had any neurologic illness or reported having a first-degree or second-degree relatives with ET or PD; (7) all subjects with apparent brain vascular or structural changes defected on T2- or T1-weighted images were discarded; and (8) all subjects met the image quality and head motion control criteria (see Supporting Information). Finally, a total of 127 ET patients and 120 age- and sex-matched HCs were recruited.

Tremor severity was assessed with the Fahn-Tolosa-Marin Tremor Rating Scale (FTM-TRS) (Fahn et al., 1993). This scale is composed of three parts: TRS part A, B and C. The TRS parts A and B were used primarily for the evaluation of tremor severity, location and the drawing and writing function of hand. The TRS-C was assessed via self-evaluation to evaluate the quality of life for ET patients. Considering a ceiling effect for severe tremor while tremor amplitude >4 cm for the TRS scale, the Essential Tremor Rating Assessment Scale (TETRAS) (Elble et al., 2012) was also adopted to assess tremor severity in our study. We also recorded the tremor frequency index from electromyography examination in ET patients. Mini-Mental State Examination (MMSE), 17-item Hamilton Depression Rating Scale (HDRS-17) and the Hamilton Anxiety Rating Scale (HARS-14) were used to briefly assess the cognitive function and mood status of all the participants, and exclude the subjects with dementia (MMSE <24), depression (HDRS-17 > 7) and anxiety (HARS-14 > 7).

2.2 | Image data acquisition and data preprocessing

All MR images were acquired using a GE Signa HdxT 3-T scanner (General Electric Medical Systems, Waukesha, WI) equipped with a standard eight-channel head coil. Rubber earplugs were used to reduce noise, and foam cushioning was used to reduce motion artifacts. During the scan time, the subjects were required to close their eyes, but not to fall asleep, and to relax their minds and move as little as possible. The resting-state functional images were collected using an echo-planar imaging (EPI) pulse sequence with the following parameters: 33 axial slices, slice thickness/gap = 4.0/0 mm,

matrix = 64×64 , TR = 2000 ms, TE = 40 ms, flip angle = 90° , FOV = 240×240 mm, and a total of 240 volumes were obtained (duration = 8 min). High-resolution 3D T1-weighted images (TR = 8.3 ms, TE = 3.3 ms, flip angle = 15° , slice thickness/gap = 1.0/0 mm, FOV = 240×240 mm, and matrix = 256×192) and T2-weighted FLAIR images (TR = 8000 ms, TE = 126 ms, TI = 1500 ms, slice thickness/gap = 5.0/1.5 mm, FOV = 240×240 mm, and matrix = 256×192) were also acquired. We did not use the T2-weighted FLAIR images for data processing, but they were used for image evaluation and data quality assessment.

All functional imaging data preprocessing was performed using the Statistical Parametric Mapping (SPM12; www.fil.ion.ucl.ac.uk/spm) and Data Processing Assistant for Resting-State fMRI (DPARSF; <http://rfmri.org/DPARSF>) programs operated on the Matlab platform. Preprocessing of the Rs-fMRI data was performed as follows: (1) removal of the first 10 time points. For scanner stabilization and the acclimation of subjects to the MR scanning environment, the first 10 volumes were discarded, and the remaining 230 time points were included in the subsequent data preprocessing; (2) slice timing correction. This was used to correct for a different acquisition time across slices in a volume; (3) realignment. This was used to realign the subsequent functional images to the first volume to correct for within-run head motions, resulting in Friston's 24 head motion parameters. These parameters were employed to assess the head movement and ensure the quality of Rs-fMRI data; (4) T1 segmentation and spatial normalization. The T1 images were co-registered to the mean Rs-fMRI data for each subject. Specifically, 3D T1-weighted images were segmented into gray matter (GM), white matter (WM) and cerebrospinal fluid (CSF) probability maps using SPM DARTEL segmentation. All the GM, WM and CSF images were resampled to isotropic 1.5-mm voxels, spatially normalized to the MNI space using both affine transformation and non-linear deformation, and later, resampled to isotropic 3-mm voxel resolution with Rs-fMRI, and the deformation field was applied to the Rs-fMRI data; (5) regressing out Friston's 24 head motion parameters (Yan et al., 2013) and the mean time series of global, WM and CSF signals; (6) spatial smoothing with a Gaussian kernel of 4 mm full width at half maximum, and (7) detrending and filtering. These steps removed the extremely low-frequency drift and the high-frequency physiological noises. For detrending, we used first-order polynomial functions; and for filtering, we adopted band-pass filtering (0.01 Hz ~ 0.08 Hz) to the time series for each voxel. FC analysis was based on the pre-processed images.

2.3 | Regions of interest and connectivity matrices

Previous studies have demonstrated that the subregions of the thalamus are associated with tremor in ET patients. For this reason, an automated anatomical labeling atlas 3 (AAL3) with thalamus parcellation was used to define the regions of interest (ROI) in our study (Rolls et al., 2020). However, some structures in the AAL3 atlas (resolution: $1 \times 1 \times 1$ mm) are so small (such as the right thalamic nucleus reuniens and ventral tegmental area) that they could not be identified in the Rs-fMRI images (resolution: $3 \times 3 \times 3$ mm). Meantime, only

ROIs >95% of voxels contained BOLD signal in >95% participants were included, and finally, 164 ROIs were defined. The mean time courses of the 164 ROIs were extracted. Then, Pearson correlation analysis was performed on the time series of each pair of ROIs, and a Fisher transformation was performed. Finally, for each subject $164 \times (164-1)/2 = 13,366$ FC values were obtained to act as input features.

2.4 | Feature selection

As the dimension of 13,366 features is so high, to avoid model overfitting and the curse of dimensionality, the feature dimension reduction was performed (Zhu et al., 2010). First, we randomly divided all subjects into a training set (70%, 172 subjects) and a testing set (30%, 75 subjects). Then, we performed a Mann-Whitney *U* test to compare each feature between ET patients and HCs, and features with *p* value less than .01 were retained. Finally, we further applied a least absolute shrinkage and selection operator (LASSO) regression model to choose the most important features for classification (Tibshirani, 1996). The LASSO performed both regularization and variable selection that compresses high-dimensional data by shrinking coefficients for weaker predictors toward zero and dropping variables from the model when their coefficients reach zero. A penalty term ($|\beta_i|$) is added to the linear regression model in LASSO which can shrink coefficients toward zero (L1 regularization). As the penalty term increases, the LASSO sets more coefficients to zero. The loss function of LASSO is as follows:

$$L = \sum_{i=1}^n (y_i - \hat{y}_i)^2 + \lambda \sum_{j=1}^p |\beta_j| \quad (1)$$

The penalization parameter λ was tuned under the criterion of minimal mean squared error (MSE) to construct the optimal subset of features via a fivefold cross-validated grid-search approach. Features with non-zero coefficients in the LASSO regression model were selected to train the classification model.

2.5 | Model fitting and validation

In this study, four classification algorithms namely support vector machine (SVM), random forest (RF), gradient boosting decision tree (GBDT) and Gaussian naïve Bayes (GNB) were employed to identify ET from HCs. SVM is a representative supervised machine-learning algorithm which has been commonly used to solve the classification of neurodegenerative diseases (Cortes & Vapnik, 1995). In this study, the optimal kernel function and two hyperparameters of the SVM (the regularization parameter *C* and kernel width parameter γ) were tuned by the grid search approach. We identified the optimal parameter combination with the highest accuracy during 10-fold cross-validation and applied this to the final model using the best parameter combination onto the testing set.

Two common types of tree-based models are gradient boosting decision tree and random forest algorithms. The random forest classifier is an ensemble method integrating all decorrelated trees to create

a final classifier (Breiman, 2001). In a random forest, there is no association between multiple independent decision trees. When a new input sample enters, it will be judged by each decision tree. At last, the classification result of the random forest is determined by the majority of prediction results voted on all decision trees. The gradient boosting decision tree is an iterative decision tree algorithm that is composed of multiple classification decision trees (Li et al., 2020). It achieves the purpose of classification by adopting an additive model and constantly reducing the residuals generated in multiple iterations. The random forest improves the performance of classification model by reducing its variance, while the gradient boosting decision tree improves the performance of model by decreasing its bias. In implementing the tree-based models, parameters were optimized for the maximum iteration number and the minimum number of samples required to split an internal node. We set the maximum number of features default value of `max_features = "auto,"` meaning that all features for a split could be used. Naive Bayes classifier is a supervised learning method based on Bayes' theorem with a naïve assumption of independence between each pair of features. Given a class variable Y and a dependent feature vector X_1 through X_n , we can get Equation 2 using Bayes' formula:

$$P(Y|X_1, \dots, X_n) = \frac{P(Y)P(X_1, \dots, X_n|Y)}{P(X_1, \dots, X_n)} \quad (2)$$

Different naive Bayes classifiers make different assumptions regarding the distribution of $P(X_i|Y)$. We used the Gaussian Naive Bayes in this study, which assumed the features had a Gaussian distribution (Equation 3):

$$P(X_i|Y) = \frac{1}{\sqrt{2\pi\sigma_Y^2}} e^{-\frac{(X_i - \mu_Y)^2}{2\sigma_Y^2}} \quad (3)$$

When training the models, we conducted hyper-parameters tuning using grid-search to discover the combination of parameters that performed best on the training set. The machine-learning workflow of model construction and validation is shown in Figure S1. These models were fitted using the training set and then assessed by applying the model to the testing set. Model performance was assessed through the following metrics: accuracy, sensitivity, specificity and area under the curve (AUC). As the random splitting of the datasets produced the variation and sampling bias, we employed a nested cross-validation method by further conducting 100 rounds of leave-group-out cross-validation (LGOVCV). Briefly, data were randomly split into training and testing sets, with 70% of subjects used to train the model, and 30% used to test the models' predictive accuracy. For each classifier, we averaged AUC, accuracy, sensitivity and specificity values from the 100 times repeated LGOVCV, which were presented as the means and standard deviations (mean \pm standard deviation [SD]). To determine whether the obtained accuracy and AUC values were significantly higher than chance, we applied permutation tests repeated 1000 times to evaluate the statistical significance of classification performance. Specifically, the p value is computed as the

fraction of predicted classification accuracies, upon permutation, that exceed the actual accuracy. Moreover, the classifier could be demonstrated to have reliable learning performance if the p value was less than .05. The above feature selection process, classification model building and optimization were implemented in Python 3.8 using the scikit-learn machine-learning library (version 1.0.2) (Abraham et al., 2014).

2.6 | Statistical analysis

The Kolmogorov–Smirnov test (K-S test) was conducted to test the normal distribution of continuous variables. The demographic and clinical data between ET and HC were compared using the two-sample t -test or Mann–Whitney U test as appropriate. All statistics were performed using SPSS with a two-tailed $p < .05$ considered significant. For any given two classification models, a statistically significant Delong test result ($p < .05$) indicates that they are significantly different. In order to investigate whether the significant discriminative RSFC features were related to the clinical tremor characteristics, a partial Pearson's correlation analysis was also conducted in the ET group.

3 | RESULTS

3.1 | Demographic characteristics

Table 1 shows the demographic and clinical information for all participants in this study. No significant difference was observed in terms of gender, age, education level and HDRS-17 score between ET patients and HCs, while a significant difference was detected for HARS-14 ($p = .0004$) and MMSE ($p = .0450$) between the two groups.

3.2 | Classification algorithms for ET and HC

The RSFC features were ranked based on selection frequency across 100 runs of 10-fold cross-validation. To better illustrate the differences in these selected features, we listed the RSFC features with selection frequency more than 70 times and the respective connected brain regions in the AAL3 template (Figure 1) and calculated the mean and SD of the selected features between the ET and HC group, respectively (Table 2). Therefore, the increasing or decreasing trend of selected RSFC features between the two groups could be viewed at the corresponding values. In addition, the brain regions related to RSFC features are shown in Figure 2.

Table 3 summarizes the detailed performances of the four classification algorithms. As we can see from the table, the performance of SVM classifier is best and achieved an accuracy of 82.8%, sensitivity of 83.7%, specificity of 81.9% and AUC of 0.902. GBDT achieved an accuracy of 79.4%, a sensitivity of 79.3%, a specificity of 79.5% and an AUC of 0.880 and RF achieved an accuracy of 78.9%, a sensitivity of 80.0%, a specificity of 77.6% and an AUC of 0.864. The naïve Bayes classifier model was less accurate (AUC, 0.793). To further

TABLE 1 Demographic and clinical features of ET and HCs

Measure	ET	HCs	Statistics	p value
Demographic				
Sample size	127	120	NA	NA
Age (years)	45.96 ± 14.35	45.61 ± 12.66	T = 0.20	.8380
Gender (M:F)	59:68	68:52	Z = -1.48	.1390
Education (years)	13.02 ± 4.53	12.13 ± 4.77	T = 1.52	.1300
Handedness (R/L)	127:0	120:0	Z = 0.00	1.0000
Cigarette smoker	33	27	Z = -0.64	.5240
Clinical of tremor				
Tremor onset (years)	33.51 ± 10.72	NA	NA	NA
Tremor duration (years)	12.45 ± 9.35	NA	NA	NA
Positive family history				
Positive	37	NA	NA	NA
Negative	90	NA	NA	NA
Alcohol sensitivity				
Positive	54	NA	NA	NA
Negative	30	NA	NA	NA
NA	43	NA	NA	NA
Tremor medication				
Propranolol	27 (40.83 ± 19.07 mg)	NA	NA	NA
Tremor symmetry				
R = L	93	NA	NA	NA
R < L	11	NA	NA	NA
R > L	23	NA	NA	NA
Tremor frequency (Hz)				
TRS-parts A&B	23.60 ± 7.94	NA	NA	NA
TRS-part C	13.00 ± 6.94	NA	NA	NA
TETRAS	21.33 ± 7.18	NA	NA	NA
TETRAS-ADL	13.55 ± 7.11	NA	NA	NA
Clinical (psychology and cognitive)				
HDRS-17	2.17 ± 1.22	2.13 ± 1.33	T = 0.20	.8440
HARS-14	2.91 ± 1.16	2.48 ± 1.76	T = 3.592	.0004
MMSE	28.71 ± 1.27	29.03 ± 1.26	T = -2.02	.0450
Head movement				
FD_power (mm)	0.01 ± 0.06	0.01 ± 0.06	T = 0.74	.4620
Scrubbed volumes	15.08 ± 7.83	15.47 ± 9.36	T = -0.36	.7230

Abbreviations: ET, essential tremor; HARS-14, 14-item Hamilton Anxiety Rating Scale; HCs, healthy controls; HDRS-17, 17-item Hamilton Depression Rating Scale; MMSE, Mini-Mental State Examination; NA, not applicable; TETRAS, Essential Tremor Rating Assessment Scale; TETRAS-ADL, Essential Tremor Rating Assessment Scale-Activities of Daily Living; TRS, Fahn-Tolosa-Marin Tremor Rating Scale.

assess the robustness of the four methods, the receiver operating characteristic (ROC) curves were shown in Figure 3.

3.3 | Correlation between selected RSFC values and clinical characteristics

The partial Pearson's correlation analysis demonstrated that six RSFC features were significantly correlated with clinical tremor

characteristics. Detailed results of the correlation analysis are presented in Figure 4. The RSFC values in Thal_VPL_R-Precentral_R ($r = .56, p < .001$) and Thal_VPL_L-Precentral_L ($r = .44, p < .001$) were positively correlated with tremor frequency in ET patients. The RSFC values between Thal_VPL_R-Cerebellum_3_R ($r = -.42, p < .001$), Cerebellum_3_R-Precentral_R ($r = -.44, p < .001$), Thal_VPL_L-Cerebellum_3_L ($r = -.44, p < .001$) and Thal_VPL_L-Cerebellum_8_L ($r = -.55, p < .001$) were negatively correlated with TRS part A&B scores in ET patients.

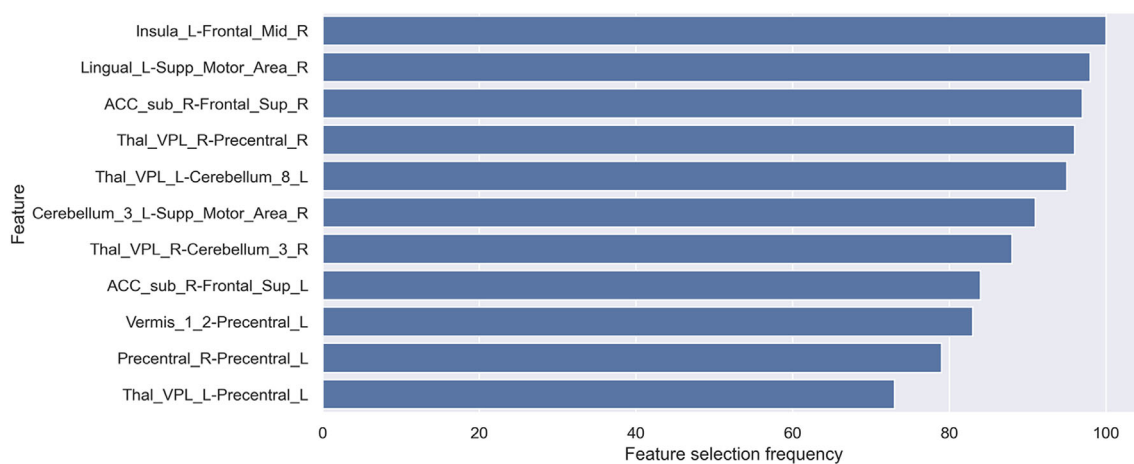


FIGURE 1 The 11 features with a selection frequency greater than 70 in 100 rounds of leave-group-out cross-validation

TABLE 2 Classification performance of different machine-learning algorithms on the testing set

Model	ACC	SEN	SPE	AUC
SVM	82.8 ± 3.8% ^a	83.7 ± 5.8%	81.9 ± 6.0%	0.902 ± 0.029 ^a
RF	78.9 ± 4.9% ^a	80.0 ± 6.4%	77.6 ± 8.9%	0.864 ± 0.045 ^a
GBDT	79.4 ± 4.7% ^a	79.3 ± 6.4%	79.5 ± 7.8%	0.880 ± 0.036 ^a
GNB	72.4 ± 7.3% ^a	71.4 ± 9.9%	79.5 ± 7.8%	0.793 ± 0.074 ^a

Abbreviations: ACC, accuracy; AUC, area under the receiver operator curve; GBDT, gradient boosting decision tree; GNB, Gaussian naïve Bayes; RF, random forest; SEN, sensitivity; SPE, specificity; SVM, support vector machine.

^a $p < .05$ under permutation test (1000 times).

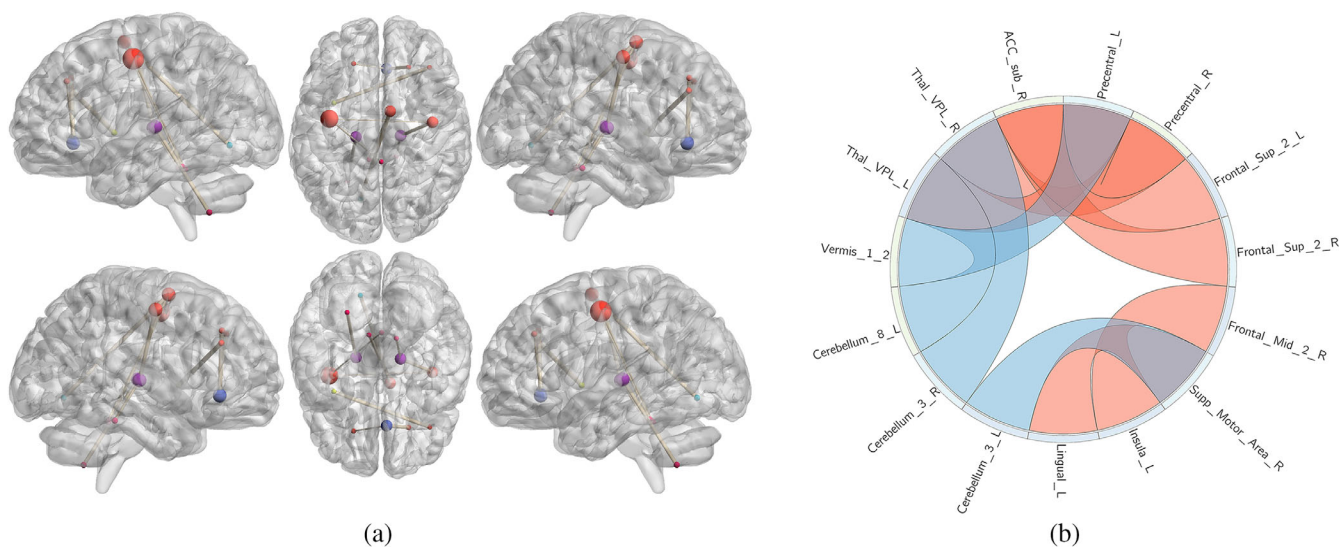


FIGURE 2 The functional connectivity map of features with selection frequency greater than 70 in 100 rounds of leave-group-out cross-validation. (a) The size of the node represents the number of connections that this brain area takes part in. The thickness of the lines between any two nodes represents the feature selection frequency. (b) The labels on the circle denote the regions of interests in AAL3 atlas as nodes in functional connectivity calculation. A red connecting line represents increased functional connectivity in essential tremor (ET), while a blue connecting line represents decreased functional connectivity in ET compared with healthy controls

4 | DISCUSSION

To the best of our knowledge, we first combined RSFC matrices data as input features with multiple machine-learning algorithms to identify

ET from HCs, and three main findings were gained: (1) All of the four machine-learning algorithms achieved good classification performance, and the SVM classifier gave the best classification performance with overall accuracy, sensitivity, specificity and AUC value at

TABLE 3 The mean, standard deviation (SD) and *p* value for selected RSFC features (with greater than 70 times) in the ET group and HC groups (ranked by the feature selection frequency)

ID	Features	ET (mean ± SD)	HC (mean ± SD)	<i>p</i> value
1	Insula_L-Frontal_Mid_R	0.4541 ± 0.2136	0.3057 ± 0.2124	.0000
2	Lingual_L-Supp_Motor_Area_R	0.4212 ± 0.2145	0.3022 ± 0.2039	.0002
3	ACC_sub_R-Frontal_Sup_R	0.3865 ± 0.2544	0.2621 ± 0.1882	.0000
4	Thal_VPL_R-Precentral_R	0.3303 ± 0.4042	0.1373 ± 0.2478	.0003
5	Thal_VPL_L-Cerebellum_8_L	0.061 ± 0.2149	0.249 ± 0.2763	.0000
6	Cerebellum_3_L-Supp_Motor_Area_R	0.3774 ± 0.2118	0.4831 ± 0.2028	.0000
7	Thal_VPL_R-Cerebellum_3_R	0.1607 ± 0.2752	0.3791 ± 0.2801	.0001
8	ACC_sub_R-Frontal_Sup_L	0.4208 ± 0.2289	0.3054 ± 0.1694	.0033
9	Vermis_1_2-Precentral_L	0.3259 ± 0.2027	0.4307 ± 0.1992	.0000
10	Precentral_R-Precentral_L	0.7901 ± 0.1464	0.6729 ± 0.1695	.0001
11	Thal_VPL_L-Precentral_L	0.3536 ± 0.3745	0.1779 ± 0.2359	.0000

Abbreviations: ET, essential tremor; HC, healthy control; RSFC, resting-state functional connectivity.

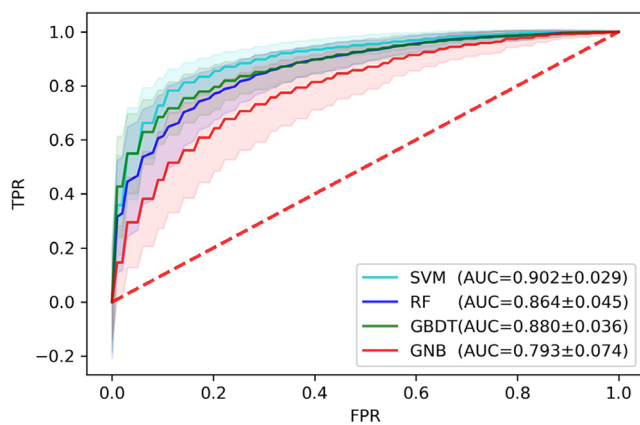


FIGURE 3 The receiver operating characteristic (ROC) curves on the testing set. AUC, area under the receiver operator curve; GBDT, gradient boosting decision tree; GNB, Gaussian naïve Bayes; RF, random forest; SVM, support vector machine; TPR, true positive rate; FPR, false positive rate.

82.8%, 83.7%, 81.9% and 0.902; (2) The high discriminative power features were mainly located in the cerebello-thalamo-motor and non-motor cortical pathway; and (3) Some of the main discriminative features could be used to partially explain the clinical tremor characteristics.

Although in the past few years, the mass-univariate RSFC analysis has made substantial progress in revealing the brain network pathogenesis in ET patients. The conventional univariate RSFC analysis methods treat each brain region as an independent area. However, these brain regions do not exist in isolation rather they are highly interconnected to constitute brain state-specific functional networks (Raichle & Mintun, 2006). Meantime, the RSFC images own a large amount of quantitative information from thousands to millions of voxels. Due to the properties of high functional interconnectivity and high dimension of the RSFC data, the univariate RSFC analysis results could not be used to predict the individual ET patients, and it also was not sensitive to reveal the spatial subtle distribution changes of these RSFC metrics. Compared to mass-univariate analysis, machine-learning

algorithms have the merits of considering all potential interactions without a predefined hypothesis and extracting new sets of data-driven features from massive input quantitative information, which overcomes the shortages of traditional univariate analysis (Pereira et al., 2009). Consistent with these above machine-learning studies, our results showed that the four machine-learning algorithms also achieved good classification performance in identifying ET from HCs.

In our study, the high discriminative power RSFC features were mainly located in the classical tremor network, including motor-related cortices, motor-thalamus (ventral posterior lateral nucleus of the thalamus) as well as the cerebellum. However, it is still debated whether the typical cerebello-thalamo-motor cortical pathway is associated with tremor in ET patients (Lenka et al., 2017; Tsuboi et al., 2021). Few studies supported that the FC changes did not only restrict to the classical tremor network but also extended to other brain regions (Tuleasca et al., 2020). Using visual feedback task fMRI (Archer et al., 2018) analysis, studies showed that BOLD amplitude in visual and parietal areas was associated with ET patients. Benito-Leon et al. (Benito-Leon et al., 2019) pointed out that changes of the RS-fMRI network organization in widespread brain regions including the thalamo-visuo-motor, salience and other extra-motor networks were related to ET patients. Our results seemed to be inconsistent with the above studies, and we speculated that the following reasons may be reasonable explanations. First, as an etiologically, clinically and pathologically heterogeneous disease, the heterogeneity of ET may yield different conclusions from different researchers, especially for small samples and absence of strict inclusion criteria. Second, the ventral posterior lateral nucleus of thalamus cannot be identified in common atlases such as the anatomical automatic labeling atlas (AAL), Harvard Oxford atlas and Brainnetome atlas (BNA), and this leads to difficulty in directly revealing the classical tremor network changes. Finally, all the above studies also revealed BOLD signal or RS-fMRI network organization changes in the typical tremor network. Therefore, our results were in line with the previous studies indeed. Meantime, compared with the previous studies, a large sample size (127 ET patients and 120 HCs) and strict inclusion (the 2018 Consensus Criteria of the Movement Disorder Society) were adopted in our studies. So, we

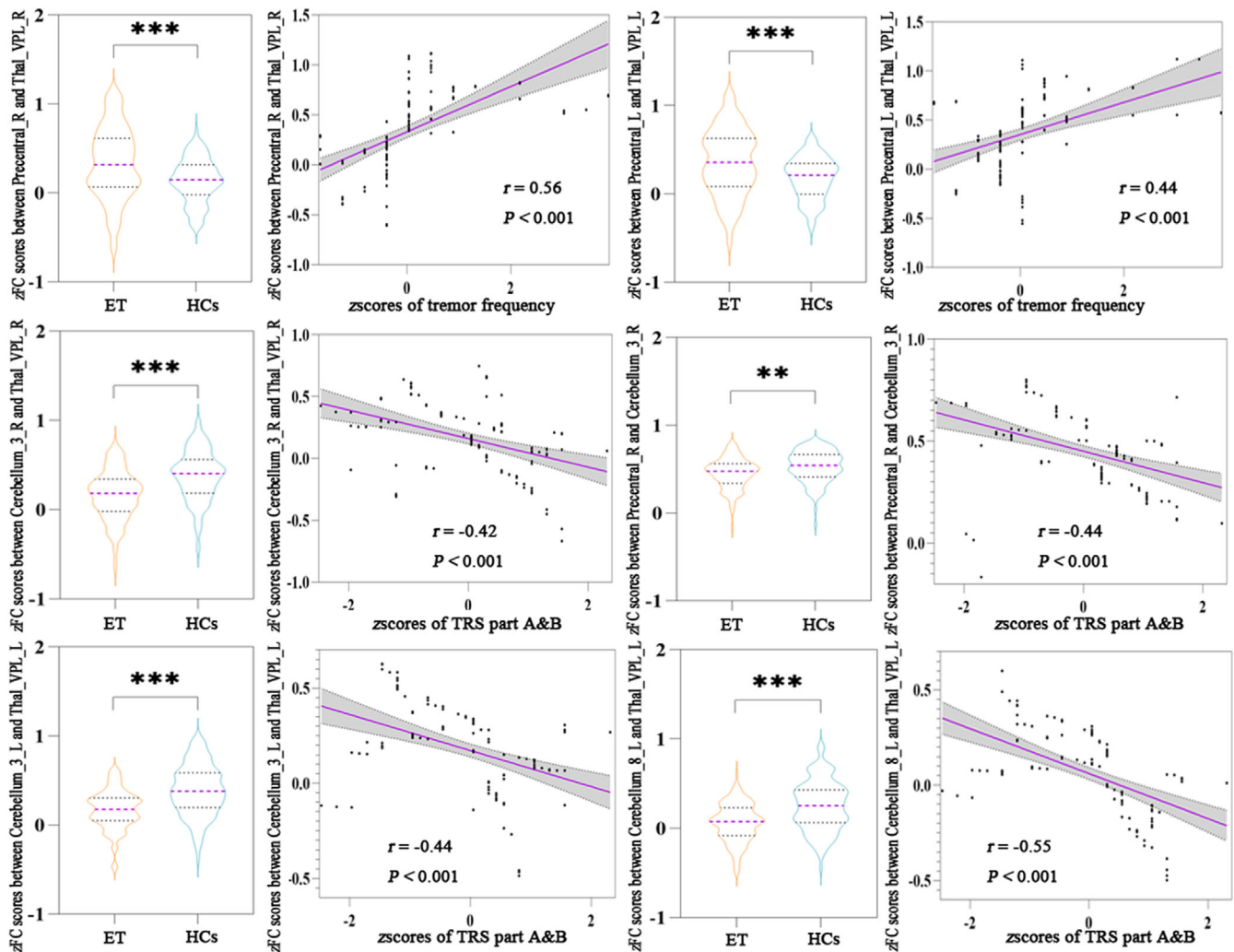


FIGURE 4 Correlation of the RSFC values across the brain regions and clinical characteristics. Violin plots displaying the mean RSFC values in the significant discriminative regions in the essential tremor (ET) and healthy control groups; scatter plots showing the correlation analysis in the ET group. *** $p < .001$, ** $p < .01$

suggest that the high discriminative power of RSFC features located in the classical tremor network further reinforces the classical tremor network pathogenesis theories in ET.

Furthermore, our results also presented that the high discriminative power RSFC features extended out the classical tremor network including non-motor cortices, such as the anterior cingulate cortex and frontal gyrus, etc. Growing evidence pointed out that the cerebellum plays an important role in the pathophysiology of ET, and the functional and neuroanatomical heterogeneity of the cerebellum (Mavroudis et al., 2022; Rajput & Rajput, 2011; Schmahmann, 2010) provide a reasonable explanation for the above results. In the presence of cerebellar dysfunction, it may not only present heterogeneous clinical symptoms, including tremor and other motor and non-motor disorders but also show the FC changes involved in cerebellar-motor and non-motor circuits. Although we applied a rigorous inclusion and obtained a highly homogeneous ET group by excluding ET patients with severe cognitive impairment, anxiety and depression, it could not

fully eliminate the influence of the above non-motor symptoms in the future, and even get rid of a compensatory state to prevent the development of these non-motor symptoms.

Although our study had several strengths, we also acknowledged some limitations. Firstly, all patients were collected from a single center at the First Affiliated Hospital of Chongqing Medical University. The classification models required further validation on larger multi-center patient samples. Secondly, this study used only whole-brain RSFC as input features to investigate whether a single indicator can be used to identify ET from HCs. Additional studies incorporating multiple metrics of fMRI or structural MRI data may be needed to test out the possibilities of multimodal machine learning in ET. Moreover, because of the lack of clinical biomarkers, the diagnosis of ET is mainly based on clinical symptoms. Therefore, to reduce the possibility of misdiagnosis, all ET patients included in the study cohort were followed up for more than 3 years and had electromyogram results for auxiliary disease diagnosis.

5 | CONCLUSION

In this study, we proposed a framework to uncover neuroimaging markers of ET based on multiple supervised machine-learning algorithms and achieved good classification performances for distinguishing ET from HCs. Furthermore, the most discriminative power features were not only confined to the typical motor networks but also extended into non-motor networks, and these features would help to understand the brain network pathogenesis mechanisms in ET.

AUTHOR CONTRIBUTIONS

Xueyan Zhang: Research project—conception, execution; statistical analysis—design, execution; manuscript preparation—writing of the first draft. **Huiyue Chen:** Research project—execution; statistical analysis—execution, review and critique; manuscript preparation—review and critique. **Xiaoyu Zhang:** Research project—execution; statistical analysis—execution, review and critique; manuscript preparation—review and critique. **Hansheng Wang:** Research project—execution; statistical analysis—execution; manuscript preparation—review and critique. **Li Tao:** Research project—conception, organization; statistical analysis—design, execution; manuscript preparation—writing of the first draft. **Wanlin He:** Research project—execution; statistical analysis—execution; manuscript preparation—review and critique. **Qin Li:** Research project—execution; statistical analysis—review and critique; manuscript preparation—review and critique. **Oumei Cheng:** Research project—execution; manuscript preparation—review and critique. **Jing Luo:** Research project—execution; manuscript preparation—review and critique. **Yun Man:** Research project—organization; statistical analysis—review and critique; manuscript preparation—review and critique. **Zheng Xiao:** Research project—organization; statistical analysis—review and critique; manuscript preparation—review and critique. **Weidong Fang:** Research project—conception, organization; statistical analysis—design, execution, review and critique; manuscript preparation—review and critique.

ACKNOWLEDGMENTS

The authors thank all participants for their participation. We also acknowledge the support of the National Natural Science Foundation of China (NSFC: 81671663) and the Natural Science Foundation of Chongqing (NSFCQ: cstc2014jcyjA10047).

CONFLICT OF INTEREST

The authors declare that there is no conflict of interest regarding the publication of this article.

DATA AVAILABILITY STATEMENT

The data that support the findings of this study are available from the corresponding author upon reasonable request.

ETHICS STATEMENT

The studies involving human participants were reviewed and approved by the Ethics Committee of the First Affiliated Hospital of

Chongqing Medical University. All subjects gave written informed consent in accordance with the Declaration of Helsinki.

ORCID

Xueyan Zhang  <https://orcid.org/0000-0002-9867-6273>

REFERENCES

- Abraham, A., Pedregosa, F., Eickenberg, M., Gervais, P., Mueller, A., Kossaifi, J., Gramfort, A., Thirion, B., & Varoquaux, G. (2014). Machine learning for neuroimaging with scikit-learn. *Frontiers in Neuroinformatics*, 8, 14. <https://doi.org/10.3389/fninf.2014.00014>
- Archer, D. B., Coombes, S. A., Chu, W. T., Chung, J. W., Burciu, R. G., Okun, M. S., Shukla, A. W., & Vaillancourt, D. E. (2018). A widespread visually-sensitive functional network relates to symptoms in essential tremor. *Brain*, 141(2), 472–485. <https://doi.org/10.1093/brain/awx338>
- Benito-León, J., Louis, E. D., Mato-Abad, V., Sánchez-Ferro, A., Romero, J. P., Matarazzo, M., & Serrano, J. I. (2019). A data mining approach for classification of orthostatic and essential tremor based on MRI-derived brain volume and cortical thickness. *Annals of Clinical Translational Neurology*, 6(12), 2531–2543. <https://doi.org/10.1002/acn3.50947>
- Benito-Leon, J., Sanz-Morales, E., Melero, H., Louis, E. D., Romero, J. P., Rocon, E., & Malpica, N. (2019). Graph theory analysis of resting-state functional magnetic resonance imaging in essential tremor. *Human Brain Mapping*, 40(16), 4686–4702. <https://doi.org/10.1002/hbm.24730>
- Bhatia, K. P., Bain, P., Bajaj, N., Elble, R. J., Hallett, M., Louis, E. D., Raethjen, J., Stamelou, M., Testa, C. M., Deuschl, G., & Tremor Task Force of the International Parkinson and Movement Disorder Society. (2018). Consensus Statement on the classification of tremors. from the task force on tremor of the International Parkinson and Movement Disorder Society. *Movement Disorders*, 33(1), 75–87. <https://doi.org/10.1002/mds.27121>
- Breiman, L. (2001). Random forests. *Machine Learning*, 45(1), 5–32.
- Cortes, C., & Vapnik, V. (1995). Support-vector networks. *Machine Learning*, 20(3), 273–297. <https://doi.org/10.1007/BF00994018>
- Elble, R., Comella, C., Fahn, S., Hallett, M., Jankovic, J., Juncos, J. L., LeWitt, P., Lyons, K., Ondo, W., Pahwa, R., Sethi, K., Stover, N., Tarsy, D., Testa, C., Tintner, R., Watts, R., & Zesiewicz, T. (2012). Reliability of a new scale for essential tremor. *Movement Disorders*, 27(12), 1567–1569. <https://doi.org/10.1002/mds.25162>
- Fahn, S., Tolosa, E., & Marín, C. (1993). Clinical rating scale for tremor. *Parkinson's Disease and Movement Disorders*, 2, 271–280.
- Fang, W., Chen, H., Wang, H., Zhang, H., Puneet, M., Liu, M., Lv, F., Luo, T., Cheng, O., Wang, X., & Lu, X. (2016). Essential tremor is associated with disruption of functional connectivity in the ventral intermediate Nucleus-Motor Cortex-Cerebellum circuit. *Human Brain Mapping*, 37(1), 165–178. <https://doi.org/10.1002/hbm.23024>
- Fang, W., Lv, F., Luo, T., Cheng, O., Liao, W., Sheng, K., Wang, X., Wu, F., Hu, Y., Luo, J., Yang, Q. X., & Zhang, H. (2013). Abnormal regional homogeneity in patients with essential tremor revealed by resting-state functional MRI. *PLoS One*, 8(7), e69199. <https://doi.org/10.1371/journal.pone.0069199>
- Lenka, A., Bhalsing, K. S., Panda, R., Jhunjhunwala, K., Naduthota, R. M., Saini, J., Bharath, R. D., Yadav, R., & Pal, P. K. (2017). Role of altered cerebello-thalamo-cortical network in the neurobiology of essential tremor. *Neuroradiology*, 59(2), 157–168. <https://doi.org/10.1007/s00234-016-1771-1>
- Li, T., Yang, K., Stein, J. D., & Nallasamy, N. (2020). Gradient boosting decision tree algorithm for the prediction of postoperative intraocular lens position in cataract surgery. *Translational Vision Science & Technology*, 9(13), 38. <https://doi.org/10.1167/tvst.9.13.38>
- Mavroudis, I., Kazis, D., Petridis, F., Chatzikonstantinou, S., Karantali, E., Njau, S. N., Costa, V., Ciobica, A., Trus, C., Balmus, I. M., &

- Baloyannis, S. J. (2022). Morphological and morphometric changes in the Purkinje cells of patients with essential tremor. *Experimental and Therapeutic Medicine*, 23(2), 167. <https://doi.org/10.3892/etm.2021.11090>
- Nicoletti, V., Cecchi, P., Pesaresi, I., Frosini, D., Cosottini, M., & Ceravolo, R. (2020). Cerebello-thalamo-cortical network is intrinsically altered in essential tremor: Evidence from a resting state functional MRI study. *Scientific Reports*, 10(1), 16661. <https://doi.org/10.1038/s41598-020-73714-9>
- Norman, K. A., Polyn, S. M., Detre, G. J., & Haxby, J. V. (2006). Beyond mind-reading: Multi-voxel pattern analysis of fMRI data. *Trends in Cognitive Sciences*, 10(9), 424–430. <https://doi.org/10.1016/j.tics.2006.07.005>
- Pereira, F., Mitchell, T., & Botvinick, M. (2009). Machine learning classifiers and fMRI: A tutorial overview. *NeuroImage*, 45(1), S199–S209. <https://doi.org/10.1016/j.neuroimage.2008.11.007>
- Prasad, S., Pandey, U., Saini, J., Ingahalikar, M., & Pal, P. K. (2019). Atrophy of cerebellar peduncles in essential tremor: A machine learning-based volumetric analysis. *European Radiology*, 29(12), 7037–7046. <https://doi.org/10.1007/s00330-019-06269-7>
- Raichle, M. E., & Mintun, M. A. (2006). Brain work and brain imaging. *Annual Review of Neuroscience*, 29, 449–476.
- Rajput, A. H., & Rajput, A. (2011). Significance of cerebellar Purkinje cell loss to pathogenesis of essential tremor. *Parkinsonism & Related Disorders*, 17(6), 410–412. <https://doi.org/10.1016/j.parkreldis.2011.05.008>
- Reich, S. G. (2019). Essential tremor. *Medical Clinics of North America*, 103(2), 351–356. <https://doi.org/10.1016/j.mcna.2018.10.016>
- Rolls, E. T., Huang, C. C., Lin, C. P., Feng, J., & Joliot, M. (2020). Automated anatomical labelling atlas 3. *NeuroImage*, 206, 116189. <https://doi.org/10.1016/j.neuroimage.2019.116189>
- Schmahmann, J. D. (2010). The role of the cerebellum in cognition and emotion: Personal reflections since 1982 on the dysmetria of thought hypothesis, and its historical evolution from theory to therapy. *Neuropsychology Review*, 20(3), 236–260. <https://doi.org/10.1007/s11065-010-9142-x>
- Tibshirani, R. (1996). Regression shrinkage and selection via the lasso. *Journal of the Royal Statistical Society: Series B (Methodological)*, 58(1), 267–288.
- Tsuboi, T., Wong, J. K., Eisinger, R. S., Okromelidze, L., Burns, M. R., Ramirez-Zamora, A., Almeida, L., Shukla, A. W., Foote, K. D., Okun, M. S., Grewal, S. S., & Middlebrooks, E. H. (2021). Comparative connectivity correlates of dystonic and essential tremor deep brain stimulation. *Brain*, 144(6), 1774–1786. <https://doi.org/10.1093/brain/awab074>
- Tuleasca, C., Bolton, T., Regis, J., Witjas, T., Girard, N., Levivier, M., & Van De Ville, D. (2020). Graph theory analysis of resting-state functional magnetic resonance imaging in essential tremor. *Human Brain Mapping*, 41(6), 1689–1694. <https://doi.org/10.1002/hbm.24900>
- Yan, C. G., Craddock, R. C., He, Y., & Milham, M. P. (2013). Addressing head motion dependencies for small-world topologies in functional connectomics. *Frontiers in Human Neuroscience*, 7, 910. <https://doi.org/10.3389/fnhum.2013.00910>
- Zhu, L., Yang, J., Song, J. N., Chou, K. C., & Shen, H. B. (2010). Improving the accuracy of predicting disulfide connectivity by feature selection. *Journal of Computational Chemistry*, 31(7), 1478–1485. <https://doi.org/10.1002/jcc.21433>

SUPPORTING INFORMATION

Additional supporting information can be found online in the Supporting Information section at the end of this article.

How to cite this article: Zhang, X., Chen, H., Zhang, X., Wang, H., Tao, L., He, W., Li, Q., Cheng, O., Luo, J., Man, Y., Xiao, Z., & Fang, W. (2023). Identification of essential tremor based on resting-state functional connectivity. *Human Brain Mapping*, 44(4), 1407–1416. <https://doi.org/10.1002/hbm.26124>